ADVANCING EARTH AND SPACE SCIENCES

Geophysical Research Letters

RESEARCH LETTER
10.1029/2026GL122492

Tracking a Rangeland Fire With Infrasound Arrays

Jacob F. Anderson[1], Madeline A. Hunt[1], Jeffrey B. Johnson[1], and Kara M. Yedinak[2]

[1]Department of Geosciences, Boise State University, Boise, ID, USA, [2]Northern Research Station, US Forest Service, Madison, WI, USA

Key Points:

- A relatively low-intensity prescribed rangeland fire in cool, moist weather produced infrasound detectable within thousands of meters
- A more distant 44 infrasound sensor array outperformed nearer 3–4 sensor arrays at identifying coherent infrasound and direction of arrival
- Fire infrasound direction of arrival follows known ignition locations, showing the potential of infrasound in wildland fire monitoring

Supporting Information:

Supporting Information may be found in the online version of this article.

Correspondence to:

J. F. Anderson,
jacobanderson152@boisestate.edu

Citation:

Anderson, J. F., Hunt, M. A., Johnson, J. B., & Yedinak, K. M. (2026). Tracking a rangeland fire with infrasound arrays. *Geophysical Research Letters*, *53*, e2026GL122492. https://doi.org/10.1029/2026GL122492

Received 18 FEB 2026
Accepted 7 JUN 2026

Abstract We present the first infrasound analyses of a rangeland fire and demonstrate infrasound's potential in monitoring wildland fires. We recorded a prescribed fire in sagebrush steppe in cool, moist conditions, using eight infrasound arrays of diverse size (3–44 sensors, 10–200 m width) and distance (0–20 km), including four arrays inside the burn area. Infrasound arrays within 2 km of fires detected coherent infrasound between 1 and 10 Hz, both during active ignitions and also while existing fires continued burning during breaks in ignitions. During periods of active ignitions, the direction of arrival estimated by a 44-sensor array closely tracked the actual locations where the helicopter was igniting vegetation. Despite being farther from the fire than four smaller arrays, the 44-sensor array performed best at identifying coherent infrasound and yielding consistent directions of arrival. Our results show infrasound's potential for tracking low-intensity wildland fires in research or hazard monitoring.

Plain Language Summary Wildland fires are hazardous and complex events that are inhospitable to ground-based measurement. Current aerial and satellite measurement platforms rely on line-of-sight techniques that are sensitive to the presence of smoke and the point of observation. By contrast, sound transmission and detection are not sensitive to the presence of smoke and can monitor sound sources in near real-time. In this study, we use infrasound (pressure waves in air) to monitor the progression of a rangeland fire. This new fire monitoring approach has the ability to capture a wider range of fire sizes, is not dependent upon line-of-sight techniques, and does not interfere with wildland fire suppression operations. Infrasound is already in wide use for monitoring other hazards, but its use in wildland fire monitoring is new. In this low-intensity rangeland fire, we detected infrasound up to about 2 km from the fires that produced it. Clusters of sensors, called infrasound arrays, were able to identify the direction to the fire and track its progress as the fires moved. This critical information, detectable for even mild fires, has the potential to aid in wildland fire monitoring and provide information across a wide range of time and space scales.

1. Introduction

Wildfire risk has increased due to factors like climate change, land management practices, invasive species, and anthropogenic ignitions (Abatzoglou & Williams, 2016; Fusco et al., 2022). The frequency, severity, and extent of wildfires is predicted to increase further over the coming decades due to hotter, drier, and windier conditions (Wasserman & Mueller, 2023). Existing fire monitoring tools, such as satellite remote sensing or aircraft-mounted sensors, present issues with obstructed visibility (from smoke or forest canopies), infrequent recording intervals, and/or limited spatial coverage (Chen et al., 2024; Viegas et al., 2008). Low-frequency pressure wave monitoring–infrasound—is relatively low-cost, unobstructed by smoke or trees, and records continuously over a large volume (Viegas et al., 2008). This could offer near-real-time information on fire activity during active wildland fires, including the potential for early warning on critical changes in fire behavior or reignition of extinguished fires.

Infrasound sees wide use for monitoring diverse natural hazards like volcanoes (Watson et al., 2022), avalanches (Johnson et al., 2021; Sovilla et al., 2025), debris flows (Belli et al., 2022), earthquakes (J. F. Anderson, Johnson, et al., 2023), and river turbulence (Schmandt et al., 2013), as well as anthropogenic processes like nuclear tests (Assink et al., 2016). Data from a single infrasound sensor provides information on source physics (e.g., Fee et al., 2017). Additionally, using an array of at least three infrasound sensors deployed near each other, scientists can estimate the direction from the array to the infrasound's source (i.e., direction of arrival) and the signal's coherency. This is useful for distinguishing which among multiple candidates is the true infrasound source (e.g., Ripepe & Marchetti, 2002) and for tracking the position and velocity of moving sources confined by topography like lahars or pyroclastic density currents (e.g., Delle Donne et al., 2014). While infrasound arrays usually contain 3–6 sensors separated by approximately 10–100 m, "large-N" arrays (defined here as containing at least tens of sensors) excel at detecting coherent infrasound in low signal-to-noise conditions as well as more accurately estimating the direction of arrival (Scamfer & Anderson, 2023).

Despite the widespread application of infrasound to natural hazard research and monitoring, its use in wildland fire monitoring is still emerging. In one early example, a fire in a wood storage facility produced infrasound that researchers detected using array methods at 1 km range, with high enough amplitude to also expect detection at approximately 10 km in the noise conditions at the time; additionally, infrasound from a gas fire was detected at a range of 12 km (Bedard & Nishiyama, 2002). These early results found dominant frequencies of 1–4 Hz and demonstrated the potential for fires to make strong infrasound that can be detected at least several km away. More recently, infrasound was recorded and analyzed in a prescribed fire in a forest understory (Marcillo et al., 2025) and a prescribed rangeland fire (this article). Although fires have multiple acoustic source processes responsible for different frequencies, fire infrasound is thought to be produced by cycles of heating air by combustion followed by buoyant rise that draws in fresh cold air, called "puffing" (Cetegen & Ahmed, 1993). In liquid pool fires, the puffing frequency depends quantitatively on the flame diameter (Fang et al., 2016); however, that relationship remains untested in wildland fires. Finally, in a recent study of a small wood pile fire, the puffing frequency observed in infrasound matched the flickering frequency observed in video recordings, with infrasound recordings spanning the 1–20 Hz band and peaked in the 1–2 Hz band, and detectable 600 m away despite the fire's small (meters-scale) size (Johnson et al., 2025).

In this study, we examine the ability of infrasound monitoring for tracking the spread of a low-intensity rangeland fire in cool, moist conditions. In particular, we compare the performance of different recording strategies including a 44-sensor array placed hundreds of meters outside the burn area, small 3–4 sensor arrays placed inside the burn area, and arrays of 5–15 sensors placed several km or tens of km from the burn area.

2. Methods

2.1. Prescribed Fire and Data Collection

We installed several infrasound arrays at Reynolds Creek Experimental Watershed (RCEW) in southwest Idaho, USA (Figure 1). One of our arrays (TOP) was a large-N array including 44 sensors in a 200 m × 130 m rectangle with approximately 20-m spacing; it was deployed on a ridge just outside and overlooking the burn area, and recorded data for about 3 months before the fire (Silber et al., 2024). Large-N infrasound arrays have previously been shown to excel at detecting infrasound with low signal-to-noise ratio, identifying the direction of arrival with high resolution, and distinguishing multiple coinciding infrasound waves arriving from different directions (J. F. Anderson, Johnson, et al., 2023; Scamfer & Anderson, 2023). In the month preceding the fire, we also deployed four arrays (JNA, JNB, JSA, JSB) alongside permanent weather stations in protected sites within the burn area (four sensors each, with spacing limited to several meters by the dimensions of the protected areas), and one array (QST) ~7 km north of the burn area (11 sensors, 60 m × 70 m). Site protection included cutting and clearing vegetation over the entire array footprint, and removing duff and organic-rich topsoil (when present) around sensors; sensors were partly covered with Firezat wrap for additional thermal protection, with an upward-facing gap for GPS reception. Additionally, we deployed two arrays for part of 6 October only: array VPT (15 sensors, 110 m × 70 m, ~15 m spacing) was deployed 2 km east of the burn area, and CHKB (5 sensors, 40 m × 30 m) was deployed ~20 km north of the burn area. Array VPT consisted of five DiGOS Datacube-3 loggers sampling at 400 samples per second connected to infraBSU infrasound sensors (Marcillo et al., 2012) made at Boise State University; all other arrays consisted of Gem infrasound loggers sampling at 100 samples per second (J. F. Anderson, Anderson, & Beschorner, 2023; J. F. Anderson et al., 2018) also made at Boise State University. We obtained coordinates for all sensors with a survey-grade GPS (accuracy finer than 1 m). At all sites, the lack of tree cover exposed sensors to significant noise from daytime air turbulence. These array locations and geometries were chosen for evaluating different recording strategies. Array TOP exemplifies a large-N array in a safe location as near the burn site as possible. Arrays JSA, JSB, JNA, JNB were deployed within the burn area in order to detect fire infrasound at shorter range and from all directions, with the tradeoffs of small size and risk of being burned. Arrays VPT, QST, and CHKB serve as tests of recording infrasound from increasingly long distances for cases when recording near the fire is impractical. As indicated by their more compact array responses, the larger arrays,

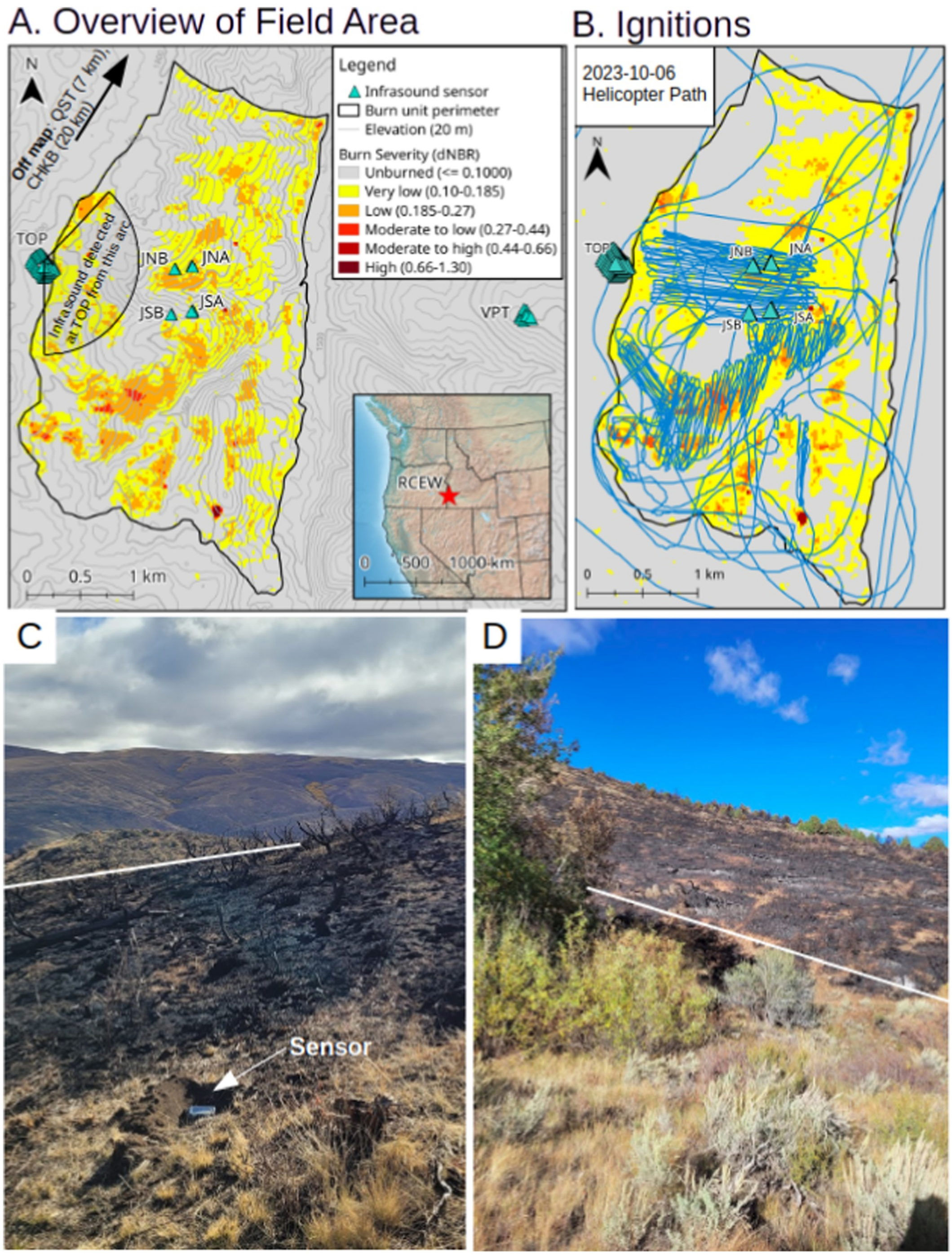

Figure 1. (a) Map showing burn area, burn severity, infrasound arrays, and infrasound directions of arrival. Arrays JNA, JNB, JSA, and JSB were inside the burn area and therefore detected infrasound from many directions, whereas fire infrasound was not detected at array VPT, QST, or CHKB due to poor signal-to-noise ratio. Burn severity was calculated using the Differenced Normalized Burn Ratio (Key & Benson, 2006) on 10-m resolution Sentinel-2 images from 28 September 2023 (pre-burn) and 8 October 2023 (post-burn). dNBR ranges from unburned (light gray) to low severity (yellow) to moderate severity (dark red). (b) Helicopter track from transponder showing attempted ignition areas over the first burn day. Note that although this paper only examines infrasound from the first day, the burn severity map includes areas burned on the second day as well. (c) Charred landscape after fire; foreground includes a sensor at array JSB (unburned due to pre-fire vegetation cutting in the array footprint and removal of duff and organic-rich soil from the sensor footprint). (d) Unburned landscape within the intended burn area, with burned landscape in background. White lines in (c, d) show boundaries between burned and unburned vegetation.

Table 1
Characteristics of the Fire's Site (From the US Bureau of Land Management Burn Plan), Surface Weather (From On-Site Sensors Operated by Reynolds Creek Experimental Watershed) and Elevated Weather (From a Radiosonde at Boise International Airport 67 km Away)

Elevation range	1,434–1,840 m
Slope	0%–25%
Area	9.35 km^2
Fuel type	GS2/TU1: Mtn big sagebrush, antelope bitterbrush, grass steppe; stands of juniper (live and cut) (SB2) and aspen
Surface temperature	15°C
Surface relative humidity	48%–56%
Surface wind speed	1–2 m/s
Surface wind direction	Mostly from N-NE
Elevated wind speed (2000–7,000 m)	5–8 m/s
Elevated wind direction	Mostly from N-NW
Burn dates	October 5: perimeter “blacklining” only; fire did not spread
	October 6: helicopter ignitions 12:46–17:55 (UTC—6:00)
	October 7: helicopter ignitions 11:04–14:20 (UTC—6:00)

especially TOP, have finer beamforming resolution (Figure S5 in Supporting Information S1) than the space-constrained small arrays inside the burn area (Figure S6 in Supporting Information S1).

RCEW is a 239-km^2 area ranging from 1,100 to 2,245 m elevation, includes several long-term hydrological and meteorological monitoring stations, and has hosted extensive environmental research since its establishment in 1960 (Seyfried et al., 2018). The prescribed fire targeted 9.35 km^2 of grassland and sagebrush steppe, with occasional felled and dried junipers. Wooded areas in the burn area included narrow riparian corridors and small aspen stands that mostly failed to burn due to the cool conditions at the time of the fire (Table 1). Much of the intended burn area failed to ignite, especially on north-facing slopes (Figure 1). Except for the dried junipers that burned quickly with observably taller flames, most of the area that did ignite burned slowly with short flames. Consequently, we consider this a rangeland fire with fuel dominated by grass and shrubs, and lower intensity than would be expected for wildland fires in drier conditions. Ignitions were performed primarily by a helicopter dropping ignition spheres (Figure 1b) and secondarily by ignitors traveling on foot using drip torches and flare guns mostly around the burn area perimeter.

2.2. Data Processing

We processed each infrasound array's data using the Python package ObsPy (Krischer et al., 2015). Preprocessing consisted of reading day-long miniSEED files, applying a sixth-order high-pass filter with a corner frequency of 0.05 Hz, and trimming the data to a time interval (06:00–18:00 local time) that allows comparing low-noise early-morning conditions, high-noise mid-day conditions before first ignition, and fire infrasound. We then looped through several one-octave frequency bands (as low as 0.125 Hz, up to 32 Hz) and performed a frequency-domain shift-and-stack beamforming analysis on each band using ObsPy's array_processing() function with 60-s non-overlapping windows. We then repeated this analysis for each array. The 4–8 Hz band had a high signal-to-noise ratio in this prescribed fire, and we focus on this band's beamforming results in this paper.

In addition to using beamforming analysis to calculate the direction of arrival, we calculated spectral characteristics of infrasound recordings. Raw power spectrograms of daytime recordings are difficult to interpret due to pervasive turbulent noise (Figure S1 in Supporting Information S1); however, because turbulent noise is incoherent among sensors, it can be reduced by stacking traces or spectra after time-shifting them according to the calculated direction of arrival. We calculate time shifts as the dot product

$$\Delta t_n = s \cdot \Delta x_n \tag{1}$$

where the slowness vector $s = (\sin(\theta)\sin(\phi), \cos(\theta)\sin(\phi), \cos(\phi))$ for estimated direction of arrival θ (0° for a wave arriving from the north) and estimated incidence angle ϕ (0° for a wave arriving from above), and Δx_n being the position vector of sensor n with respect to some fixed reference point for the array. Then, the stacked spectrum for an array is

$$Y_{\text{stack}}(f) = \frac{1}{N}\sum_{n=1}^{N} Y_n(f)\exp(2\pi i f \Delta t_n) \tag{2}$$

where $Y_{\text{n}}(f)$ is the complex Fourier transform of the detrended, windowed 60-s time series of sensor n for frequency f, N is the number of sensors, i is the imaginary unit, and Δt_n is the time delay from Equation 1 at sensor n for the slowness vector being tested. We then calculate the semblance spectrum—a measure of signal coherence across the array—as the stacked spectrum normalized by the sum of power spectra of all sensors in the array:

$$S(f) = \frac{Y_{\text{stack}}(f)\,Y_{\text{stack}}(f)^*}{\frac{1}{N}\sum_{n=1}^{N} Y_n(f)\,Y_n(f)^*} \tag{3}$$

where multiplication of spectra by their complex conjugates (denoted by asterisks) results in a purely real result. Semblance varies strictly between 0 and 1; however, when sensors record pure uncorrelated noise, semblance is approximately $1/N$, which complicates the comparison of semblance values from arrays of different sizes. To remove this bias, we calculate "adjusted semblance" as

$$S_a(f) = \frac{N}{N-1}\left(S(f) - \frac{1}{N}\right) \tag{4}$$

As with unadjusted semblance, $S_a(f) = 1$ for a signal that can be explained perfectly as a single plane wave crossing the array with no noise; unlike unadjusted semblance, $S_a(f)$ has an expected value of zero and can actually take small negative values for pure uncorrelated noise regardless of N. We plot adjusted semblance in Figure S1B in Supporting Information S1 as spectra, and plot the evolution of the adjusted semblance spectrum over time in Figures 2k–2l as spectrogram-like images in order to show times and frequencies at which coherent infrasound signal is present.

3. Results

3.1. Pre-Fire Infrasound

Pre-fire infrasound observations follow a common pattern seen in previous large-N array analysis (e.g., Scamfer & Anderson, 2023): coherent early-morning background noise dominated by low-amplitude infrasound waves arriving from far away, followed at about 10:00 by incoherent noise dominated by air turbulence (details and spectra in Figure S1 in Supporting Information S1). Accordingly, consistent directions of arrival can be identified in the early morning data, but not in the late morning data (Figure 2). Although low-amplitude infrasound waves from far away are probably still present after 10:00, they are masked by higher-amplitude turbulence; consequently, infrasound waves recorded after 10:00 would need to have high enough amplitude to be detected over the incoherent turbulent noise.

3.2. Fire Infrasound

Ignitions began at 12:46 local time on 6 October, mostly by a helicopter dropping ignition spheres. The helicopter focused on sub-areas within the burn area, remaining within a sub-area before moving to the next one (Figure 1). Ignition spheres ignited vegetation within tens of seconds of being dropped, with an additional delay for the fire to grow large and spread. So, we expect that some portion of the fire infrasound sources would follow the helicopter's path with a delay of minutes to tens of minutes, and therefore plot the direction from array to helicopter as an indicator of directions where infrasound generation is expected (Figure 3). We note that some infrasound may also arise from long-lasting fires ignited within the burn area perhaps hours previously, or from fires ignited by workers on the ground (a likely explanation for the directions observed around 14:30–15:00, when workers on the

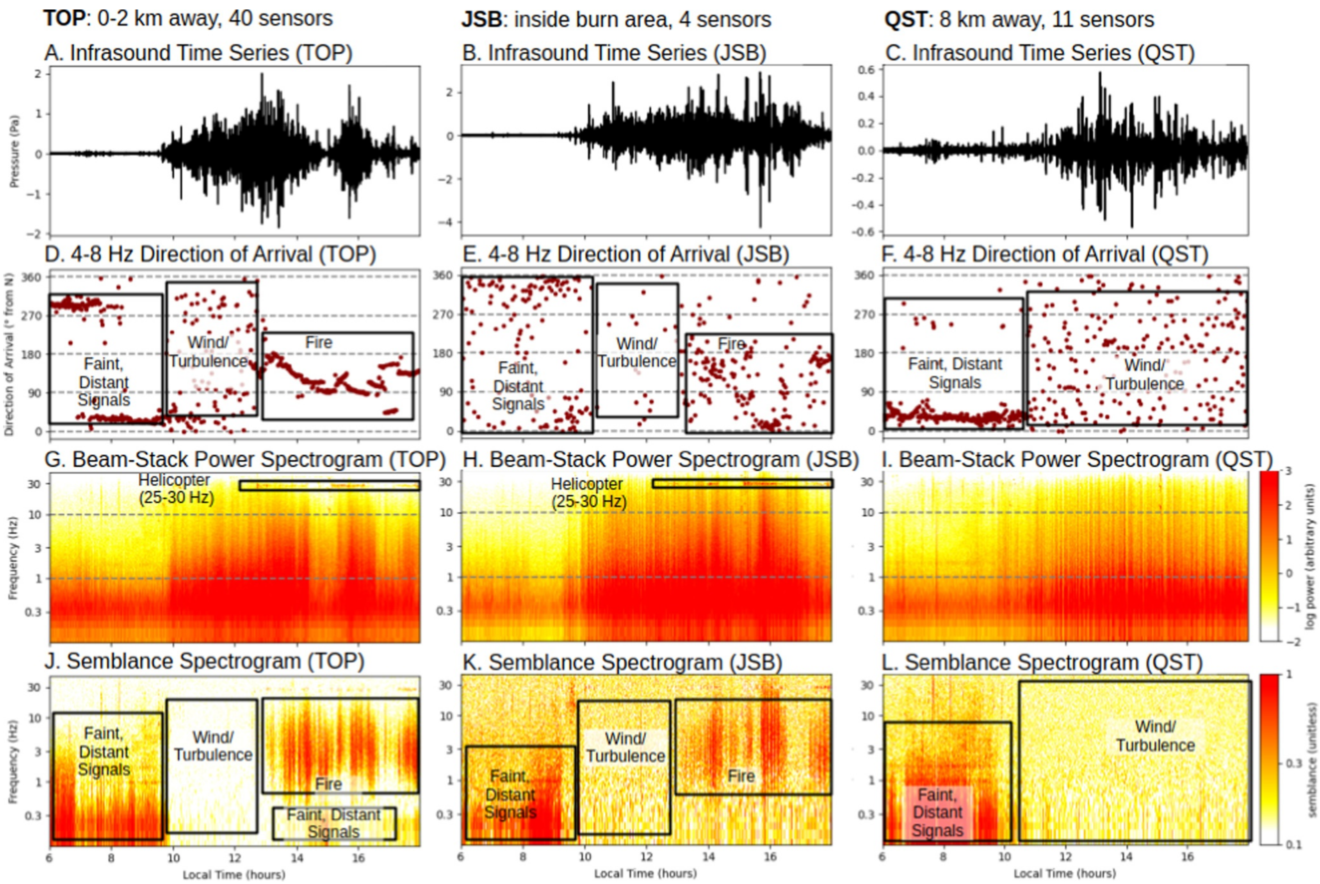

Figure 2. Analyses of infrasound data from three arrays with different geometries and locations. (a–c) Raw infrasound waveforms with no array processing performed. (d–f) Evolution of direction of arrival over time. (g–l) Evolution of frequency content over time as measured by power (d–f) and semblance (g–i). All three arrays detect distant night-time signals clearly, but the more distant station QST does not detect fire signals. Although fire signals are not distinguishable from pre-fire turbulent noise in power spectrograms, fire signals show up most clearly in semblance data between about 1 and 10 Hz after the 12:46 ignition at arrays TOP and JSB. Helicopter infrasound is only apparent in a narrow band from 25 to 30 Hz.

ground were observed conducting ignitions in the valley between JSA, JSB, JNA, and JNB). Additionally, the helicopter did not drop ignition spheres at every point on its path; in addition to trips to refuel, some of its flight consisted of short excursions for reconnaissance.

Fire infrasound is apparent in both the semblance spectrogram and directions of arrival immediately after the first ignitions (Figures 2a–2c and 2j–2l) despite not being visible in infrasound time series or power spectrograms (Figures 2g–2i). These observations are clearest at the large-N array TOP (in accordance with its fine beamforming precision shown by its compact array response, Figure S5 in Supporting Information S1), present but less clear at the small array JSB, and absent at the intermediate-sized distant array QST (10 km away). Additionally, the other small arrays within the burn area JSA, JNA, and JNB detected fire infrasound, while the more distant arrays VPT (2 km) and CHKB (20 km) did not (Figures S3 and S4 in Supporting Information S1). Although coherent infrasound is present over a wide frequency band spanning at least 1–10 Hz (Figures 2j–2l), we focus on the 4–8 Hz band when calculating direction of arrival because of its high semblance and because its relatively short wavelengths facilitate precise direction of arrival estimation. Comparison of direction of arrival to helicopter position demonstrates the dominant but not exclusive role of helicopter-performed ignitions in the infrasound; as predicted, the infrasound generally follows the helicopter's position with a short delay during the burn period. However, pre-ignition helicopter flights (10:00–10:30) lack infrasound, the helicopter's excursions from the area being ignited do not appear in the infrasound (e.g., at 14:20), and detections from the TOP array continue when the helicopter is absent for refueling (14:30–15:00, 16:30–17:00) (Figure 3). Along with the limited frequencies affected by the helicopter (Figure 2), these indicate that the helicopter does not create

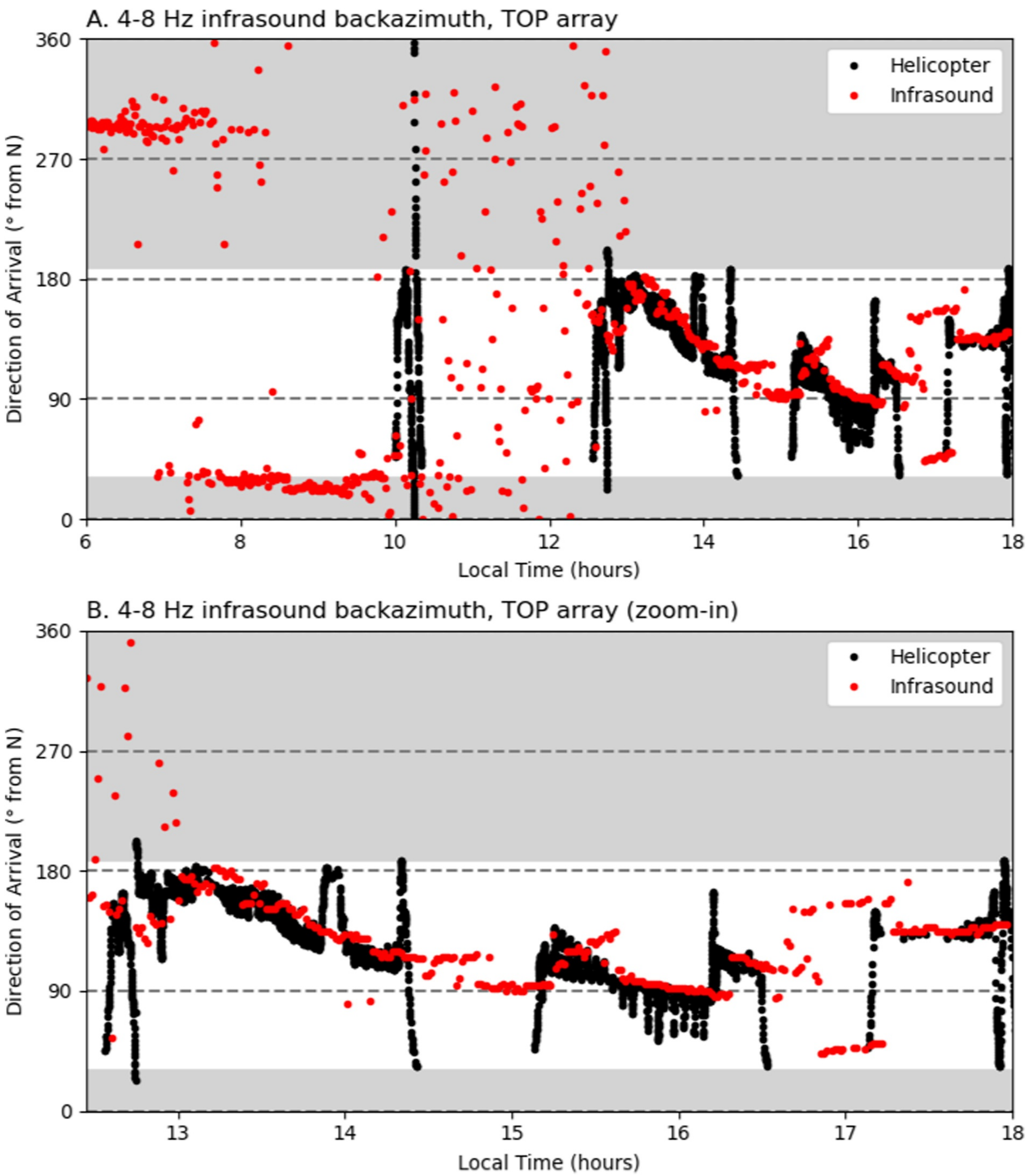

Figure 3. (a) Comparison of actual direction-to-helicopter (from TOP array to the helicopter's transponder) to infrasound direction of arrival. (b) Detail of burn period. Some overlap between helicopter position and direction of arrival is expected (and seen) because the most intense burning at a given time often occurs due to helicopter ignitions; however, some burning is not associated with recent helicopter passes and some helicopter activity is not associated with ignitions. White/gray background indicates directions inside/outside the burn area.

meaningful noise in the band used here to track fire. Contrasting with the 4–8 Hz band attributed to the fire, no time delay is observed between the helicopter's actual position and directions of arrival of the 25–32 Hz band attributed to it (Figure S2 in Supporting Information S1).

4. Discussion

This low-intensity prescribed fire produced infrasound that was detected at distances of hundreds to thousands of meters using infrasound array methods. The low density of infrasound monitoring in the western US (typical spacing of tens to hundreds of km between arrays) means that for rangeland fires of similar intensity to this one, few fires would be close enough to permanent infrasound arrays to be monitored effectively by them. Effective infrasound monitoring of fires like this would therefore require installation of a temporary telemetered infrasound network near a fire. The amount of field effort required for this can be manageable because self-contained infrasound instruments can be installed quickly (our 44-sensor TOP array took two workers approximately 45 min to set up after reaching the site). For real-time monitoring use, telemetry (e.g., cell modems) and a real-time data-processing system would be required, similar to what commercial services for monitoring avalanche infrasound have developed, and real-time signal classification or post-processing of beamforming results may be warranted to prevent false alarms. On the other hand, infrasound might be more powerful from a fire that is more intense (due to stronger infrasound-producing fluctuations in heat release rate), larger (due to superposition of waves produced in different parts of the fire), or with a linear front facing toward or away from the sensor (due to constructive interference of waves traveling similar distances to the sensor). In such cases, fire infrasound might be detected at longer distances, including by permanent monitoring stations. We note that very large and powerful fires might significantly alter local atmospheric conditions and thereby refract infrasound in unexpected ways, possibly even refracting infrasound waves away from arrays that they would normally reach. However, we expect such effects to be insignificant in low-intensity fires like this one. Topographic obstructions like ridges may also obstruct infrasound and should be considered when deciding infrasound array placement.

Although the low amplitude of the fire infrasound meant that it could not be discerned above daytime background noise in waveforms or power spectrograms, signals were coherent in the 1–10 Hz band (similar to the pile fire recorded by Johnson et al., 2025), and beamforming the 4–8 Hz band gave directions of arrival that agreed with the directions to the burn area and the ignition helicopter's track. Infrasound detections continued even when the helicopter left for refueling, indicating that infrasound arose not just from places newly ignited by the helicopter, but also from areas that continued burning long after being ignited or were ignited by personnel on the ground while the helicopter was away.

The good performance that was achieved by arrays placed within and adjacent to the 2.5 × 4 km burn area contrasts with the inability of a 15-element array (VPT) to detect fire infrasound at a range of 2–5 km, and highlights the importance of improving the signal-to-noise ratio to extend the feasible distance of fire infrasound monitoring. Two common means of mitigating noise from daytime air turbulence and wind—placing sensors in tree cover or focusing on night-time signals—are unsuitable for rangeland fire monitoring, where the most important activity occurs during the day and tree cover is scarce. Wind noise reduction systems for infrasound exist (e.g., Walker & Hedlin, 2010), but were not used in this study due to their cost and the effort required to deploy them in large numbers. Identifying low-cost, portable, easy-deploy wind noise reduction systems could help make fire infrasound monitoring work at longer distances, thereby making it more compatible with operational constraints in a dynamic active wildfire environment. Our data set was not impaired by other noise sources; in particular, the helicopter's signals fell far outside the 4–8 Hz band of interest and did not interfere with fire infrasound analysis. Different types of helicopters have been found to produce narrow-band signals within the 4–8 Hz range in other studies; however, the signals could be removed effectively using notch filters (Johnson et al., 2021).

Finally, although three-element and four-element arrays succeeded in detecting fire infrasound and identifying directions of arrival, our large-N array outperformed them at identifying coherent infrasound and yielding consistent directions of arrival, despite being farther away from most of the burn area. It also succeeds in identifying multiple infrasound sources from different directions (e.g., Figure 3, 16:30–17:15). This agrees with past work demonstrating the advantages of arrays with tens of sensors in detecting and locating infrasound, particularly in low signal-to-noise environments or wavefields with multiple simultaneous acoustic sources (J. F. Anderson, Johnson, et al., 2023; Scamfer & Anderson, 2023) and suggests that large-N arrays should be part of future fire infrasound monitoring campaigns. In particular, future work using multiple large-N arrays could track the position of dominant fire infrasound sources by finding where the arrays' back-azimuths intersect.

5. Conclusions

We recorded infrasound from a prescribed rangeland fire that burned with relatively low intensity due to cool, moist conditions and sparse fuel load. The fire produced infrasound that was detected at ranges of approximately 0–3 km, with dominant frequencies in the 1–10 Hz range, similar to past studies of wood fires. Although the infrasound's low amplitude meant it was not clearly visible in time series or power spectra, array processing revealed coherent signal over the 1–10 Hz band. Beamforming analysis yielded direction-of-arrival estimates that mostly followed the track of the helicopter performing the ignitions and fell within the burn area. Of the arrays used in the study, a 44-sensor "large-N" array yielded particularly high-quality directions of arrival and comprehensive detections of coherent infrasound during the burn period. The helicopter's noise did not interfere with fire infrasound analysis. Daytime wind/turbulent noise masked fire infrasound signals at longer distances, indicating that wind screens may be required for effective long-distance monitoring of low-intensity fires like this one. Like other hazards for which it is used, infrasound monitoring offers the potential for both research and operational monitoring of wildfires.

Conflict of Interest

The authors declare no conflicts of interest relevant to this study.

Availability Statement

The dataset is archived on Boise State's ScholarWorks repository (J. F. Anderson & Hunt, 2026). Code for figures is available as a Zenodo repository (J. Anderson, 2025).

Acknowledgments
We thank D. Huber, O. Walsh, V. Porter, and Z. Cram for helping collect infrasound data and providing meteorological data, and L. Okeson and D. Osterkamp for informative discussions on the RCEW fire and potential infrasound applications. US Forest Service award #23-JV-11111135-067 funded this work.

References

Abatzoglou, J. T., & Williams, A. P. (2016). Impact of anthropogenic climate change on wildfire across western U.S. forests. *Proceedings of the National Academy of Sciences of the United States of America*, *113*(42), 11770–11775. https://doi.org/10.1073/pnas.1607171113

Anderson, J. (2025). ajakef/RCEW_fire_infrasound_paper: 20251204 [Software]. *Zenodo*. https://doi.org/10.5281/zenodo.17822632

Anderson, J. F., Anderson, K. S., & Beschorner, T. (2023). gemlog: Data conversion for the open-source Gem infrasound logger. *Journal of Open Source Software*, *8*(86), 5256. https://doi.org/10.21105/joss.05256

Anderson, J. F., & Hunt, M. A. (2026). Infrasound from Prescribed Burn in Reynolds Creek Experimental Watershed, ID, USA [Software]. *Boise State University Infrasound Data Repository*. Retrieved from https://scholarworks.boisestate.edu/infrasound_data/17/

Anderson, J. F., Johnson, J. B., Bowman, D. C., & Ronan, T. J. (2018). The Gem infrasound logger and custom-built instrumentation. *Seismological Research Letters*, *89*(1), 153–164. https://doi.org/10.1785/0220170067

Anderson, J. F., Johnson, J. B., Mikesell, T. D., & Liberty, L. M. (2023). Remotely imaging seismic ground shaking via large-N infrasound beamforming. *Communications Earth & Environment*, *4*(1), 399. https://doi.org/10.1038/s43247-023-01058-z

Assink, J. D., Averbuch, G., Smets, P. S. M., & Evers, L. G. (2016). On the infrasound detected from the 2013 and 2016 DPRK's underground nuclear tests. *Geophysical Research Letters*, *43*(7), 3526–3533. https://doi.org/10.1002/2016gl068497

Bedard, A. J., & Nishiyama, R. T. (2002). Infrasound generation by large fires: Experimental results and a review of an analytical model predicting dominant frequencies. In *IEEE international geoscience and remote sensing symposium* (Vol. 2, pp. 876–878). IEEE. https://doi.org/10.1109/IGARSS.2002.1025715

Belli, G., Walter, F., McArdell, B., Gheri, D., & Marchetti, E. (2022). Infrasonic and seismic analysis of debris-flow events at Illgraben (Switzerland): Relating signal features to flow parameters and to the seismo-acoustic source mechanism. *Journal of Geophysical Research: Earth Surface*, *127*(6), e2021JF006576. https://doi.org/10.1029/2021jf006576

Cetegen, B. M., & Ahmed, T. A. (1993). Experiments on the periodic instability of buoyant plumes and pool fires. *Combustion and Flame*, *93*(1–2), 157–184. https://doi.org/10.1016/0010-2180(93)90090-P

Chen, Y., Morton, D. C., & Randerson, J. T. (2024). Remote sensing for wildfire monitoring: Insights into burned area, emissions, and fire dynamics. *One Earth*, *7*(6), 1022–1028. https://doi.org/10.1016/j.oneear.2024.05.014

Delle Donne, D., Ripepe, M., De Angelis, S., Cole, P. D., Lacanna, G., Poggi, P., & Stewart, R. (2014). Chapter 9 thermal, acoustic and seismic signals from pyroclastic density currents and Vulcanian explosions at Soufriere Hills Volcano, Montserrat. *Geological Society, London, Memoirs*, *39*(1), 169–178. https://doi.org/10.1144/M39.9

Fang, J., Jiang, C., Wang, J., Guan, J., Zhang, Y., & Wang, J. (2016). Oscillation frequency of buoyant diffusion flame in crosswind. *Fuel*, *184*, 856–863. https://doi.org/10.1016/j.fuel.2016.07.084

Fee, D., Izbekov, P., Kim, K., Yokoo, A., Lopez, T., Prata, F., et al. (2017). Eruption mass estimation using infrasound waveform inversion and ash and gas measurements: Evaluation at Sakurajima Volcano, Japan. *Earth and Planetary Science Letters*, *480*, 42–52. https://doi.org/10.1016/j.epsl.2017.09.043

Fusco, E. J., Balch, J. K., Mahood, A. L., Nagy, R. C., Syphard, A. D., & Bradley, B. A. (2022). The human–grass–fire cycle: How people and invasives co-occur to drive fire regimes. *Frontiers in Ecology and the Environment*, *20*(2), 117–126. https://doi.org/10.1002/fee.2432

Johnson, J. B., Anderson, J. F., Marshall, H. P., Havens, S., & Watson, L. M. (2021). Snow avalanche detection and source constraints made using a networked array of infrasound sensors. *Journal of Geophysical Research: Earth Surface*, *126*(3), e2020JF005741. https://doi.org/10.1029/2020jf005741

Johnson, J. B., Anderson, J. F., & Yedinak, K. (2025). Infrasound produced by a small pile fire. *Applied Acoustics*, *231*, 110559. https://doi.org/10.1016/j.apacoust.2025.110559

Key, C. H., & Benson, N. C. (2006). Landscape assessment (LA). In D. C. Lutes, R. E. Keane, J. F. Caratti, C. H. Key, N. C. Benson, S. Sutherland, et al. (Eds.), *FIREMON: Fire effects monitoring and inventory system. General Technical Report RMRS-GTR-164-CD* (p. 164). US Department of Agriculture, Forest Service, Rocky Mountain Research Station.

Krischer, L., Megies, T., Barsch, R., Beyreuther, M., Lecocq, T., Caudron, C., & Wassermann, J. (2015). ObsPy: A bridge for seismology into the scientific Python ecosystem. *Computational Science & Discovery*, *8*(1), 014003. https://doi.org/10.1088/1749-4699/8/1/014003

Marcillo, O., Johnson, J. B., & Hart, D. (2012). Implementation, characterization, and evaluation of an inexpensive low-power low-noise infrasound sensor based on a micromachined differential pressure transducer and a mechanical filter. *Journal of Atmospheric and Oceanic Technology*, *29*(9), 1275–1284. https://doi.org/10.1175/jtech-d-11-00101.1

Marcillo, O., Lees, J. M., Yedinak, K., Bourne, K., Potter, B., Flanagan, S., et al. (2025). Acoustic observations of a prescribed burn. *Applied Acoustics*, *235*, 110657. https://doi.org/10.1016/j.apacoust.2025.110657

Ripepe, M., & Marchetti, E. (2002). Array tracking of infrasonic sources at Stromboli volcano. *Geophysical Research Letters*, *29*(22), 2076. https://doi.org/10.1029/2002GL015452

Scamfer, L. T., & Anderson, J. F. (2023). Exploring background noise with a large-N infrasound array: Waterfalls, thunderstorms, and earthquakes. *Geophysical Research Letters*, *50*(24), e2023GL104635. https://doi.org/10.1029/2023gl104635

Schmandt, B., Aster, R. C., Scherler, D., Tsai, V. C., & Karlstrom, K. (2013). Multiple fluvial processes detected by riverside seismic and infrasound monitoring of a controlled flood in the Grand Canyon. *Geophysical Research Letters*, *40*(18), 4858–4863. https://doi.org/10.1002/grl.50953

Seyfried, M., Lohse, K., Marks, D., Flerchinger, G., Pierson, F., & Holbrook, W. S. (2018). Reynolds creek experimental watershed and critical zone observatory. *Vadose Zone Journal*, *17*(1), 1–20. https://doi.org/10.2136/vzj2018.07.0129

Silber, E. A., Bowman, D. C., Carr, C. G., Eisenberg, D. P., Elbing, B. R., Fernando, B., et al. (2024). Geophysical observations of the 24 September 2023 OSIRIS-REx sample return capsule re-entry. *arXiv*, *2407*, 02420. https://doi.org/10.3847/PSJ/ad5b5e

Sovilla, B., Marchetti, E., Kyburz, M. L., Köhler, A., Huguenin, P., Calic, I., et al. (2025). The dominant source mechanism of infrasound generation in powder snow avalanches. *Geophysical Research Letters*, *52*(2), e2024GL112886. https://doi.org/10.1029/2024gl112886

Viegas, D. X., Pita, L. P., Nielsen, F., Haddad, K., Calisti Tassini, C., D'Altrui, G., et al. (2008). Acoustic and thermal characterization of a forest fire event. In W. M. Hao (Ed.) *Remote sensing of fire: Science and application* (p. 708904). https://doi.org/10.1117/12.794601

Walker, K. T., & Hedlin, M. A. H. (2010). A review of wind-noise reduction methodologies. In A. Le Pichon, E. Blanc, & A. Hauchecorne (Eds.), *Infrasound monitoring for atmospheric studies* (pp. 141–182). Springer.

Wasserman, T. N., & Mueller, S. E. (2023). Climate influences on future fire severity: A synthesis of climate–fire interactions and impacts on fire regimes, high-severity fire, and forests in the western United States. *Fire Ecology*, *19*(1), 43. https://doi.org/10.1186/s42408-023-00200-8

Watson, L. M., Iezzi, A. M., Toney, L., Maher, S. P., Fee, D., McKee, K., et al. (2022). Volcano infrasound: Progress and future directions. *Bulletin of Volcanology*, *84*(5), 44. https://doi.org/10.1007/s00445-022-01544-w